Journal Pre-proof

Pullulan microneedle patches for the efficient transdermal administration of insulin envisioning diabetes treatment

Daniela F.S. Fonseca (Investigation) (Methodology) (Writing - original draft) (Writing - review and editing), Paulo C. Costa (Investigation) (Resources) (Writing - review and editing) (Funding acquisition), Isabel F. Almeida (Investigation) (Resources) (Writing - review and editing) (Funding acquisition), Patrícia Dias-Pereira (Investigation) (Resources) (Writing - review and editing), Inês Correia-Sá (Resources) (Writing - review and editing), Verónica Bastos (Investigation) (Writing - review and editing), Helena Oliveira (Resources) (Methodology) (Writing - review and editing) (Funding acquisition), Margarida Duarte-Araújo (Writing - review and editing), Manuela Morato (Writing - review and editing), Carla Vilela (Investigation) (Writing - review and editing) (Supervision), Armando J.D. Silvestre (Conceptualization) (Resources) (Writing - review and editing) (Supervision) (Funding acquisition), Carmen S.R. Freire (Conceptualization) (Resources) (Writing - review and editing) (Supervision) (Funding acquisition)

Pullulan microneedle patches for the efficient transdermal administration of insulin envisioning diabetes treatment

Daniela F. S. Fonseca,[a] Paulo C. Costa,[b] Isabel F. Almeida,[b] Patrícia Dias-Pereira, [c] Inês Correia-Sá,[d] Verónica Bastos,[e] Helena Oliveira,[e] Margarida Duarte-Araújo,[f] Manuela Morato,[g] Carla Vilela,[a] Armando J. D. Silvestre,[a] Carmen S. R. Freire[a*]

[a] CICECO – Aveiro Institute of Materials, Department of Chemistry, University of Aveiro, 3810-193 Aveiro, Portugal

[b] UCIBIO, REQUIMTE, MedTech - Laboratory of Pharmaceutical Technology, Department of Drug Sciences, Faculty of Pharmacy, University of Porto, Porto, Portugal

[c] Institute of Biomedical Sciences Abel Salazar, ICBAS-UPorto, University of Porto, Porto, Portugal

[d] Department of Plastic, Aesthetic, Reconstructive and Aesthetic Surgery, Centro Hospitalar de S. João, 4200-319 Porto, Portugal

[e] Department of Biology &CESAM, University of Aveiro, 3810-193 Aveiro, Portugal

[f] LAQV/REQUIMTE, Department of Immuno-Physiology and Pharmacology, Abel Salazar Institute of Biomedical Sciences (ICBAS), University of Porto, Porto, Portugal

[g] LAQV/REQUIMTE, Laboratory of Pharmacology, Department of Drug Sciences, Faculty of Pharmacy, University of Porto, Porto, Portugal

* Corresponding author: Carmen S. R. Freire, Email: cfreire@ua.pt

Graphical abstract
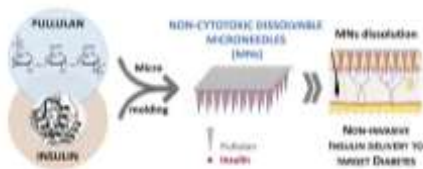
Highlights:

- Dissolvable pullulan microneedles were successfully prepared by solvent casting

- Pullulan-insulin microneedles successfully penetrate through the skin

- Storage at 4, 20 and 40 ℃ maintained the secondary structure of insulin

- Pullulan microneedles deliver 87% of insulin, 120 min after insertion.

- Pullulan-insulin microneedles are non-cytotoxic towards human keratinocyte cells

Abstract

The present study reports the fabrication of dissolvable microneedle (MN) patches using pullulan (PL), a water-soluble polysaccharide with excellent film-forming ability, for the transdermal administration of insulin, envisioning the non-invasive treatment of diabetes. PL MNs patches were successfully prepared by micromolding and revealed good thermal stability (Td_{max}=294 °C) and mechanical properties (> 0.15 N.needle^{-1}), penetrating skin up to 381 μm depth, as revealed by *in vitro* skin tests. After application into human abdominal skin *in vitro*, the MNs dissolved within 2 h releasing up to 87% of insulin. When stored at 4, 20 and 40 ℃ for 4 weeks, insulin was able to retain its secondary structure, as shown by circular dichroism spectropolarimetry. The prepared PL MNs were non-cytotoxic towards human keratinocytes, being suitable for skin

application. These findings suggest that PL MNs have potential to deliver insulin transdermally, thus avoiding its subcutaneous administration.

Keywords: pullulan; polysaccharides; insulin; microneedles; transdermal drug delivery.

1. Introduction

Diabetes mellitus is a group of chronic metabolic disorders characterized by signs and symptoms of hyperglycemia, *viz.* high blood glucose levels (Tuomi et al., 2014). Diabetes mellitus is currently recognized as one of the largest epidemics in the world and its incidence is rising. In 2015, it was estimated that 415 million people had diabetes and the latest reports predict that over 642 million people will be affected by 2040 (Ogurtsova et al., 2017). Although there are different types of diabetes mellitus, namely type 1, type 2 and gestational diabetes are the most prevalent (Tuomi et al., 2014). Type 2 diabetes is by far the most prevalent form of this disease, accounting for more than 90% of all cases, being responsible for the current global health problem (DeFronzo et al., 2015).

The incidence of insulin-dependent type 1 diabetes is lower, but it is raising particularly in children younger than 5 years of age. The impairment of insulin secretion due to autoimmune destruction of pancreatic beta cells and/or peripheric insulin action resistance leads to chronic hyperglycemia and subsequent vascular and neuronal complications, that impact patients disease burden (Rydén et al., 2016). Therefore, insulin therapy is currently the most effective treatment to achieve normoglycemia in type 1 diabetes, minimizing related complications (DeFronzo et al., 2015; Tuomi et al., 2014). Insulin is usually administered subcutaneously (SC) due to its poor oral bioavailability (Saffran, Pansky, Budd, & Williams, 1997), but SC injections are

3

associated with increased inflammation and infection risk, as well as poor patient compliance (Asche, Shane-McWhorter, & Raparla, 2010). In addition, repeated injections around the same spot may lead to skin thickening and poor glycemic control, resulting in suboptimal management of diabetes (Derraik et al., 2014).

To overcome these drawbacks, minimally invasive alternative routes have been investigated, including oral, pulmonary, nasal, buccal, peritoneal and transdermal administration (Carmo et al., 2014; Shah, Patel, Maahs, & Shah, 2016). In particular, transdermal administration of insulin has gained a great momentum in the past few decades owing to its easy self-application coupled with improved patient adherence (Economidou, Lamprou, & Douroumis, 2018; Jin, Zhu, Chen, Ashfaq, & Guo, 2018; Matteucci et al., 2015; Shah et al., 2016). More recently, attention has been paid to the use of microneedles (MNs) as a simple and minimally invasive method for the self-administration of this pharmaceutical. MNs have the ability to accelerate insulin absorption, due to the richness in small vessels that the *stratum papillare* of the skin presents (X. Chen et al., 2018; Ling & Chen, 2013; Ross, Scoutaris, Lamprou, Mallinson, & Douroumis, 2015).

The first report concerning the use of MNs for insulin administration dates back to 2003, and showed that stainless steel devices provided therapeutic efficacy by reducing blood glucose levels in diabetic rats (McAllister et al., 2003). Since then, MNs for insulin administration have been sculped using several different materials, with polymers being the most extensively explored (Fonseca, Vilela, Silvestre, & Freire, 2019). Nowadays, there is an increasing interest in the production of biopolymeric devices, including MNs (Fonseca et al., 2019), due to their intrinsic biocompatibility, safety, low cost and sustainability. In this sense, literature reports the use of several biopolymers namely hyaluronic acid (Liu et al., 2012), starch and gelatine (Ling &

4

Chen, 2013), alginate (Yu et al., 2017), dextrin (Ito, Hagiwara, Saeki, Sugioka, & Takada, 2006), poly-γ-glutamic acid (M.-C. Chen, Ling, & Kusuma, 2015) and chondroitin sulphate (Ito, Yamazaki, Sugioka, & Takada, 2010) in MNs for insulin administration (Narayan, 2014).

Pullulan (PL) is a non-ionic natural exopolysaccharide produced by yeasts and composed of α-(1→6) maltotriose residues. This biopolymer displays interesting properties regarding biomedical purposes, namely non-toxicity, water solubility, production of low viscosity solutions, excellent film forming ability, adhesiveness and good mechanical performance (Ram S. Singh, Saini, & Kennedy, 2008). Furthermore, PL is emerging as an economic alternative to other natural gums of marine and plant origin (Mishra, Suneetha, & Rath, 2011; Suneetha, Sindhuja, & Singh, 2010). During the past few years, PL has been explored for the development of different materials for a panoply of applications (Ram S. Singh et al., 2008; Ram Sarup Singh, Kaur, Rana, & Kennedy, 2017), including functional packaging (Silva, Vilela, Almeida, Marrucho, & Freire, 2017), tissue engineering (Amrita, Arora, Sharma, & Katti, 2015; Ram Sarup Singh, Kaur, Rana, & Kennedy, 2016) and also drug delivery (DD) (Huang et al., 2018; Tao et al., 2018). The demand for easy-to-use insulin administration justifies the need for more effective DD systems and the study of PL MNs for insulin administration will be offset by the benefit of those who suffer with diabetes.

Our research team has been interested in the use of PL for the design of bio-based materials for different applications (Fernandes et al., 2014; Silva et al., 2017), and obtained promising preliminary results on the use of polysaccharides, including PL, for the fabrication of MNs (Freire et al., 2019). So, in the current study, PL dissolvable MNs were prepared by micromolding and characterized in terms of morphology, mechanical properties, thermal stability, humidity stability and explored for

5

incorporation and delivery of insulin. The DD efficiency was demonstrated *in vitro* using human skin samples. In order to confirm their safety for skin applications the biocompatibility of PL MNs was tested *in vitro* in human keratinocytes.

2. Materials and methods

2.1. Chemicals and materials

Pullulan (PL, 98%, MW 272 kDa) was purchased from B&K Technology Group (China). Insulin (from bovine pancreas, ≥ 25 U mg^{-1}, MW 5.8 kDa), sodium phosphate dibasic ($\geq 99.0\%$), sodium phosphate monobasic ($\geq 99.0\%$) were purchased from Sigma-Aldrich (Sintra, Portugal). Sodium chloride ($\geq 99.0\%$) was acquired from Fluka (Sigma-Aldrich, Germany). Hydrochloric acid (37%) was purchased from Acros Organics (New Jersey, USA). Ultrapure water (Type 1, 18.2 MΩ cm at 25 °C) was obtained using a Milli-Q$^®$ Integral Water Purification System (Merck, Darmstadt, Germany).

2.2. Fabrication of microneedles

Pyramidal PL microneedle patches (size 8×8 mm^2, arrays 15×15, needle height 550 μm, needle base 200 μm, needle pitch 500 μm) were produced by solvent casting using female molds of polydimethylsiloxane (PDMS) (Micropoint Technologies Pte Ltd., Singapore). Firstly, different amounts of PL were dissolved in ultrapure water, under constant stirring overnight, to obtain solutions with distinct concentration, namely 6, 9, 12, 15, 18 and 24% (w/v). Density (ρ) and dynamic viscosity (η) measurements of PL solutions were carried out using an automated SVM3000 Anton Paar rotational Stabinger viscometer-densimeter in the 10 to 80 ºC temperature range and at atmospheric pressure (≈ 0.1 MPa). The density absolute uncertainty is $\pm 5\times10^{-4}$ g cm^{-3}, the dynamic viscosity relative uncertainty $\pm 1\%$ and the temperature relative uncertainty

is ± 0.02 ℃ (Bhattacharjee, Lopes-da-Silva, Freire, Coutinho, & Carvalho, 2015). Then, approximately 40 µL of each PL solution was added to the PDMS mold and centrifuged (Hettich® Rotofix 32A) at 6000 rpm during 30 min to guarantee that the PL solution filled the pyramidal holes. Afterwards, approximately 60 µL of the same polymer solution were placed on the centrifuged layer and casted at 30 ℃ overnight.

To prepare insulin-loaded MNs (each PL MNs patch incorporated 12.4 IU insulin), a two-step casting process was adopted, as described elsewhere (Ling & Chen, 2013). First, insulin (2.7 mg) was dissolved into 0.3 mL of 0.01 M aqueous solution HCl and incorporated into the 24% (w/v) PL solution (0.5 mL). Approximately 40 µL of the drug-loaded PL was applied to the PDMS mold as the first layer and centrifuged. This step was repeated twice. A second layer of PL without insulin was then placed on the centrifuged first layer, followed by further centrifugation and solvent drying, according to the experimental conditions previously described to produce pure PL MNs. Finally, the PL 24% + Insulin MN patches were gently peeled off from the master molds and placed in a desiccator until further use.

2.3. Characterization of pullulan microneedle patches

2.3.1. Morphological characterization of microneedles

The obtained PL MNs were examined using a stereomicroscope (Nikon SMZ25, Tokyo, Japan) and microscope images were captured with a camera (SRH Plan Apo 2, Tokyo, Japan). Magnification power of the ocular lens was 5× and magnification of the objective lens was 5×, giving a total magnification of 25×. Image processing was performed using NIS Elements Imaging Software.

The morphological analysis of MNs was performed using scanning electron microscopy (SEM). Micrographs were obtained using a high voltage microscope

(HITACHI SU 70) operated at 4.0 kV. Samples were previously coated with carbon using an EMITECH K950 coating system.

2.3.2. Mechanical characterization and preliminary insertion test using a model system

Mechanical axial compressive tests were performed using a TA.XT2 Texture Analyser (Stable Micro Systems Ltd., Haslemere, UK). The MN patches were placed on the flat rigid surface of a stainless-steel base plate. An axial force, perpendicular to the axis of the array, was applied at a constant speed of 0.01 mm s^{-1}. The force was measured when the moving sensor touched the uppermost point of the needles. Then, the texture analyser recorded the force required to move the mount as a function of needle displacement (Park, Allen, & Prausnitz, 2005).

For preliminary insertion studies, Parafilm® (Bemis Company Inc., Soignies, Belgium) was folded into eight layers to simulate the thickness of excised skin, following a simple method previously reported (Larrañeta et al., 2014). The MN arrays were then inserted into the Parafilm® layers, using the texture analyser by applying a force of 40 N for 30 seconds. To measure the insertion ratio and depth, each layer of Parafilm® was examined under the microscope and the number of holes counted.

The three samples providing the highest insertion rate (MNs prepared with 15, 18 and 24% PL) were selected for compression tests using different weights, from 450 to 1800 g per patch.

2.3.3. Thermogravimetric analysis (TGA)

TGA of selected samples, namely insulin, PL 24% and PL 24% + Insulin MNs, was carried out with a SETSYS Setaram TGA analyser (SETARAM Instrumentation,

France) equipped with a platinum cell. Samples (5 mg) were heated from room temperature up to 800 ºC at a constant rate of 10 ºC.min^{-1} under a nitrogen flow.

2.3.4. Fourier transform infrared- Attenuated total reflection (FTIR-ATR) spectroscopy

FTIR-ATR spectra were obtained on a Perkin-Elmer FT–IR System Spectrum BX spectrophotometer (Perkin-Elmer Inc., USA) equipped with a single horizontal Golden Gate ATR cell. To obtain each spectrum, 64 scans were acquired in the 4000–500 cm^{-1} range, with a resolution of 4 cm^{-1}.

2.3.5. Humidity stability testing

To study the stability of the PL-based MNs towards humidity, PL 24% and PL 24% + Insulin MNs were stored at a high relative humidity (RH) environment, namely 75% RH. This condition was achieved by placing a saturated sodium chloride solution into a container. MNs were removed at pre-determined intervals, their weight was measured and the variation in MNs weight was determined and expressed in percentage.

2.3.6. Conformational stability of insulin under storage

PL 24% + Insulin MNs were stored at 4, 20 and 40 ºC for 1, 2, 3 and 4 weeks, and changes in the secondary structure of insulin were investigated by circular dichroism (CD) spectropolarimetry using a Jasco 1500 spectrophotometer, equipped with a Peltier system for temperature control. For that, stored MNs were dissolved in ultrapure water and the spectra were recorded at 20 ºC between 190 and 260 nm, at a 100 scans speed, time of 1s and 1 nm bandwidth. Each spectrum was obtained by subtracting the appropriate blank media from the experimental spectrum and was collected by averaging three spectra.

2.4. In vitro skin insertion

Human abdominal skin tissue was obtained from female donors submitted to an abdominoplasty at *Centro Hospitalar de São João* (Porto, Portugal), after signing the respective informed consent. Approval of the Ethics Committee of *Hospital de São João* was obtained. Skin was obtained after cosmetic surgery, transported under refrigerated conditions and followed removal of the adipose tissue by blunt dissection using a scalpel (blade number 24). Then, the skin surface was washed, dried using a cotton swab, wrapped in aluminium foil and stored in a freezer at -20 °C until further use (Trovatti et al., 2011).

Prior to the insertion experiments, the skin was defrosted and cut into 25 mm diameter circles using a biopsy punch. Skin samples were then placed in a sealed Petri dish, on top of a cotton pad embedded in phosphate buffered saline for 1 hour to prevent dehydration. The skin samples were fixed into a rigid support using hypodermic needles and the MN arrays placed on their surface. The MNs were pressed against skin with a force of 40 N for 30 seconds using the TA.XT2 Texture Analyser (Stable Micro Systems, Ltd., Haslemere, UK). Then, the MN arrays were peeled off and the area of compression exposed to China ink for 1 min to identify the perforation sites. Residual ink was wiped from skin samples, which were then processed for histological examination. To prepare histological specimens, skin samples were embedded in Bouin's solution, fixed in 10% formalin, dehydrated and embedded in paraffin wax. Serial 7 μm thick sections were cut from each block using a pfm Rotary 3006 EM automated microtome. The skin sections were stained with haematoxylin and eosin and analysed using a Nikon Eclipse E600 microscope to determine the penetration depth (M.-C. Chen, Ling, Lai, & Pramudityo, 2012).

2.5. In vitro insulin delivery

PL 24% + Insulin MNs were inserted into *ex vivo* human abdominal skin samples and secured using tape. The skin was subsequently placed in a sealed Petri dish on top of a cotton pad embedded in phosphate buffered saline for 2 h. At specified time intervals, the patches were removed from the skin samples. To determine the loading amount and residual amount of insulin in MNs, the patches were dissolved in DI water with stirring at 4 °C. The amount of insulin delivered into the skin was calculated by subtracting the amount of the peptide remaining in the MNs after insertion and on the skin surface using tape, from the amount originally introduced in the arrays at each sampling point (M.-C. Chen et al., 2012).

To determine the amount of insulin in PL MNs, the absorbance of a stock solution was scanned between 250 and 310 nm using a UV-Vis Spectrophotometer Shimadzu UV-1800 and the absorption maximum was determined at 276 nm. The stock standard solution of insulin was prepared in 0.01 M HCl to a concentration of 468 μg mL^{-1}. Working standard solutions were prepared from the stock standard solution and a calibration curve ($y = 1.438x - 0.045$, r^2=0.996) was constructed in the range of 184, 221, 265, 318, 381, 395, 408, 423 and 452 μg mL^{-1} for insulin (n=3).

2.6. In vitro cell viability assays

The HaCaT cell line, a nontumorigenic immortalized human keratinocyte cell line, was purchased from Cell Lines Services (Eppelheim, Germany) and all manipulation and growth were performed and adapted to meet CLS recommendations. HaCaT cells were aseptically grown in Dulbecco's modified Eagle's medium, supplemented with 10% fetal bovine serum (FBS), 2 mM L-glutamine, 1% penicillin-streptomycin (10,000

11

U mL^{-1}), and 1% fungizone (250 U mL^{-1}) (Gibco, Life Technologies, Grand Island, NY, USA), at 37 °C in a humidified atmosphere with 5% CO_2, as previously described (Ascenso et al., 2016). Cells were daily observed for confluence and morphology using an inverted phase-contrast Eclipse TS100 microscope (Nikon, Tokyo, Japan). Cell viability was determined by the colorimetric 3-(4,5 dimethyl-2-thiazolyl)-2,5-diphenyl tetrazolium bromide (MTT) assay (Mosmann, 1983). Cells were seeded in 96 wells plates at 9000 and 6000 cells *per* well for 2 and 24 h exposure, respectively. Cells were exposed to PL and insulin-loaded MNs dissolved into culture medium at 30 and 150 μg.well^{-1} (defined previously by evaluation of 5-300 μg well^{-1}, data not shown) and then further incubated for 2 and 24 h. HaCaT cells exposed to control medium were used as a negative control. At the end of the incubation time, 50 μL of MTT (at a concentration of 1 g L^{-1}) were added to each well and incubated for 4 h at 37 °C in 5% CO_2 humidified atmosphere. After that, culture medium with MTT was removed and replaced by 150 μL of DMSO and the plate was placed in a shaker for 2 h in the dark to completely dissolve the formazan crystals. The samples absorbance (*Abs*) was measured with a BioTek Synergy HT plate reader (Synergy HT Multi-Mode, BioTeK, Winooski, VT) at 570 nm with blank corrections. Data was analysed by a one-way ANOVA followed by a Holm-Šídák test to evaluate the significance between the different MNs and cell viability was calculated with respect to control cells.

2.7. *Statistical analysis*

Statistical analyses were performed using GraphPad Prism Software (GraphPad Software Inc., San Diego, CA, USA). Data is presented as the mean values ± standard error. A Student's paired *t*-test was used for comparisons between data points and multiple data sets between groups were analysed with a one-way analysis of variance

(ANOVA) followed by a Tukey's post hoc test, when necessary. For all comparisons, a difference of $p < 0.05$ was regarded as statistically significant.

3. Results and discussion

The strategy followed in the present work involved the preparation of PL solutions with different concentrations, namely 6, 9, 12, 15, 18 and 24% (w/v), followed by the fabrication of MNs by solvent casting, as illustrated in Fig. 1(a). The morphological characteristics, size and shape, and the mechanical performance of this set of MNs were assessed aiming to select the best MNs for the incorporation of insulin (Fig. 1(b)). Afterwards, the feasibility of using insulin-loaded MNs for the administration of this drug, was inferred via *in vitro* insertion tests and transdermal delivery in *ex vivo* human skin. Finally, the biocompatibility of these MNs was tested to evaluate their safety.
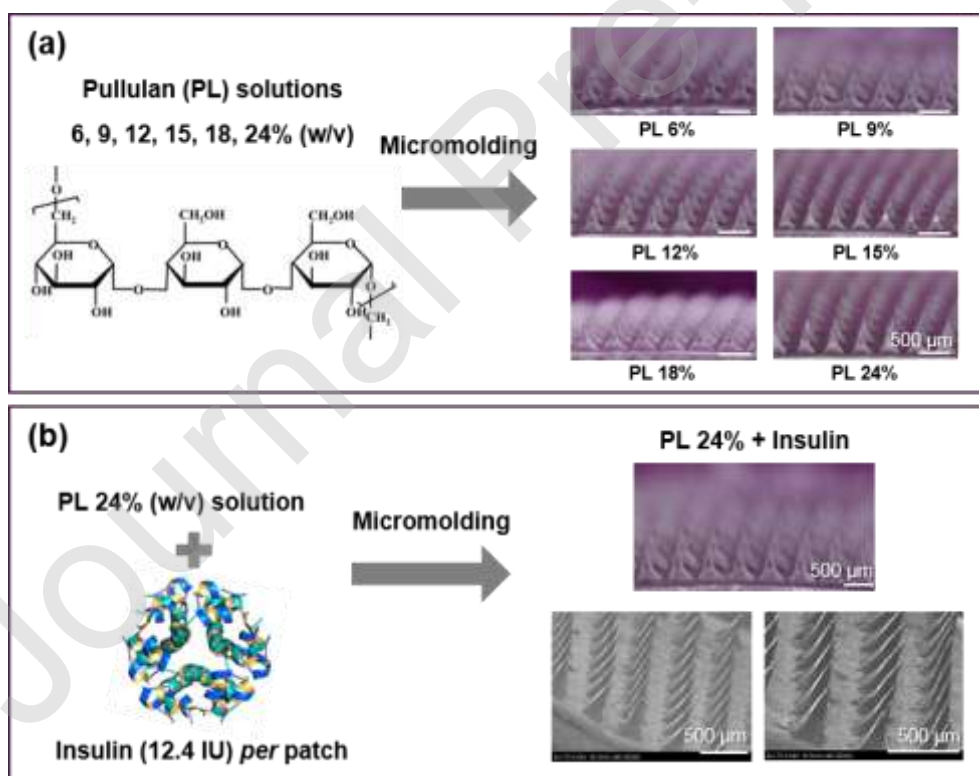
Fig. 1. (a) Schematic representation and optical micrographs of PL MNs fabricated with 6, 9, 12, 15, 18 and 24% (w/v) PL solutions, and (b) schematic representation, and optical and scanning electron micrographs of PL 24% + Insulin MNs.

3.1. Preparation and characterization of the PL dissolvable MNs patches

The preparation of MNs was carried out with pyramidal master molds (over conical ones) because they provide needles with higher mechanical strength, due to their larger cross-sectional area at the same base diameter (Lee, Park, & Prausnitz, 2008). In addition, micromolding by solvent casting was used to produce MNs owing to its simple processing coupled with low-cost and mass production potential at room temperature (Fonseca et al., 2019).

Firstly, PL solutions with 6, 9, 12, 15, 18 and 24% (w/v) were characterized in terms of density and viscosity (Fig. 2), given that these two parameters play important roles in polymer flowability and largely influence fabrication of micro-patterned polymeric devices (Fonseca et al., 2019). At 20 ºC, the viscosity of the PL solutions ranged from 18 mPa s to 1148 mPa s, and the density varied between 1.01 g cm^{-3} and 1.07 g cm^{-3} for solutions of 6% and 24%, respectively, which confirms that these parameters increase with the polymer content. Therefore, all solutions proved to be suitable for MNs fabrication by micromolding considering the density and viscosity measurements (Fonseca et al., 2019).
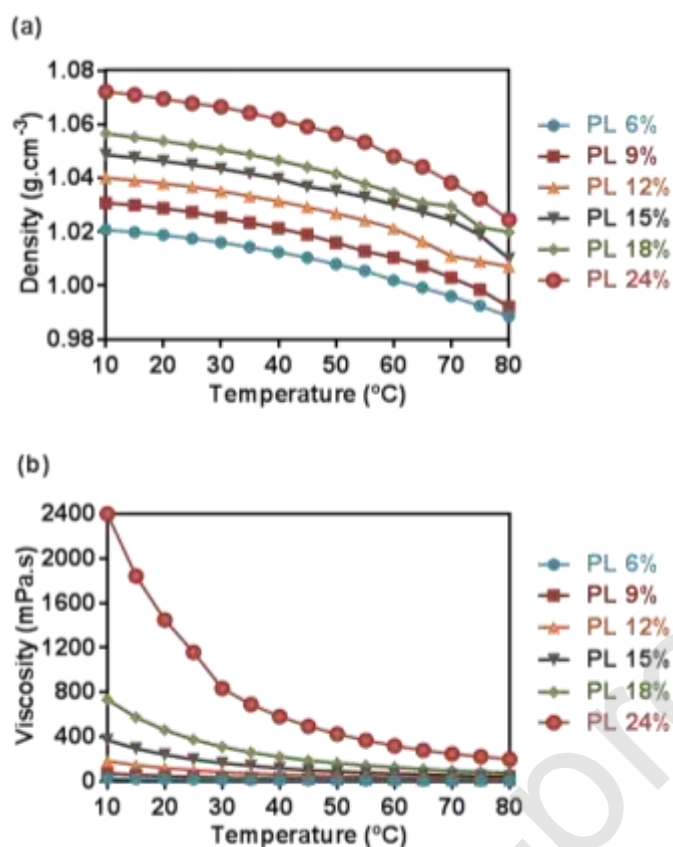
Fig. 2. Density (a) and viscosity (b) of PL aqueous solutions with concentration of 6, 9, 12, 15, 18 and 24 % (w/v).

Pullulan MN arrays containing 225 needles (15×15) with pyramidal shape and sharp tips (≈ 3-15 μm) were successfully replicated for all PL solutions (Fig. 1(a)). The optical micrographs (Fig. 1(a)) unveiled a homogeneous morphology, together with a smooth and crack-free surface for all PL MNs. Therefore, the solvent-casting micromolding is indeed an attractive and scalable approach for MNs fabrication using PL solutions from 6% to 24% (w/v).

Table 1 displays the detailed dimensions of the MNs fabricated with the different aqueous PL solutions. The base width of the MNs is around 200 μm and the needle pitch is around 500 μm, which reveals the successful replication of the master structure. The needle's height ranges from 445±13 μm to 500±14 μm, and no statistical

15

differences were found between PL 6% and 9%, 12% and 15%, 15% and 18%, and 18% and 24%. These data show that the increase in PL concentration leads to an increase in the average height of the corresponding MNs. The slight differences in MNs height, particularly for the MNs obtained from less concentrated solutions, when compared with the dimensions of the master mold, is certainly related with the solvent evaporation, ultimately leading to the decrease in needle's height. In this case, height reduction is 17-22%, 16-22%, 9-17%, 7-16%, 8-13% and 6-11% for MNs prepared with 6, 9, 12, 15, 18 and 24% PL, respectively, which agrees with results reported for other biopolymeric MNs. For instance, MNs fabricated with alginate and modified with 3-aminophenylboronic acid and hyaluronic acid, using 700 μm depth master molds, reproduced microstructures of 650 μm height (7.1% reduction) (Yu et al., 2017). Also, alginate/maltose MNs prepared using 800 μm depth master molds obtained structures with 730 μm height (8.8% reduction) (Zhang, Jiang, Yu, Liu, & Xu, 2018).

The as-prepared PL MNs display similar aspect ratios, ranging between 2.23±0.07 and 2.50±0.07, which is in line with their comparable dimensions (Table 1). In literature, it is reported that MNs with similar aspect ratio display similar mechanical properties, which allow us to expect no significant differences between the different MNs obtained in this study (Fonseca et al., 2019).

Table 1. Detailed dimensions of the MNs fabricated using PL solutions with different concentrations (from 6 to 24% w/v).

Measurements (n=75)[a]	PL 6%	PL 9%	PL 12%	PL 15%	PL 18%	PL 24%
Height (μm)	445 ± 13	446 ± 18	478 ± 221	484 ± 24	490 ± 14	500 ± 14
Base width (μm)	201 ± 3	201 ± 2	202 ± 4	203 ± 6	202 ± 4	201 ± 3

Tip-to-tip distance (μm)	500 ± 1	500 ± 1	500 ± 1	500 ± 1	500 ± 1	500 ± 1
Aspect ratio	2.23 ± 0.07	2.23 ± 0.09	2.39 ± 0.11	2.42 ± 0.12	2.45 ± 0.07	2.50 ± 0.07

[a] Measurements performed at 15 random needles selected from 5 different MNs arrays for each PL concentration.

3.2. Mechanical evaluation and preliminary insertion studies of PL MNs patches

MNs should resist skin insertion without bending or buckling, which will allow the delivery of drugs into the deepest skin layers and reach the bloodstream. In this study, the mechanical evaluation of the MNs arrays was performed by axial compression using a universal test machine. The profiles of force *versus* displacement after an axial force load are displayed in Fig. 3(a).

The results show that all samples present the same mechanical behavior, with no abrupt discontinuity upon application of an axial force load. Instead, there is a continuous and gradual increase in force, which indicates a gradual deformation of the PL MNs without breaking, as depicted in Fig. 3(a). This mechanical profile is comparable to that reported for other biopolymers MNs, namely chitosan (M.-C. Chen et al., 2012) or carboxymethylcellulose (Lee et al., 2008). Furthermore, the force *vs.* displacement values are on the same range of that registered for these two biopolymers. The PL MNs produced in this study exhibited a force from 0.3-0.53 N/needle at 0.2 mm displacement, whereas chitosan and carboxymethylcellulose MNs exhibited forces from 0.2 to 0.4 N/needle and up to 0.6 N/needle, respectively (M.-C. Chen et al., 2012; Lee et al., 2008). These values overcome the threshold value of 0.15 N.needle^{-1} reported for skin insertion using other microneedles (Davis, Landis, Adams, Allen, & Prausnitz, 2004), which demonstrates the suitability of these PL MNs for skin insertion.

17

The skin insertion ability of these MN arrays was further investigated in a skin model setup composed of eight layers of Parafilm®, where an average force of 40 N was applied to each patch for 30 seconds. According Fig. 3(b), all patches perforated the first and seconds layers of Parafilm®, but only the ones prepared with 15-24% of PL were able to reach the third layer. This third layer corresponds to a penetration depth of 381 μm, which is an indication that these PL MNs may reach the skin dermis (Fig. 3(c)).

Afterwards, the MN patches that reach higher insertion depths in the skin model (i.e. PL 15, 18 and 24%) were selected to perform compression tests using different weights. In general, it was observed that a higher compression force and PL content originates higher reductions in the MNs height. The height reductions were all in the range of 5-25%, but the results are not statistically significant among MN samples fabricated from 15 to 24% (w/v) PL. Based on these data, the MNs prepared with the PL solution of 24% (w/v), presented the highest insertion and, thus, were selected for the incorporation of insulin.
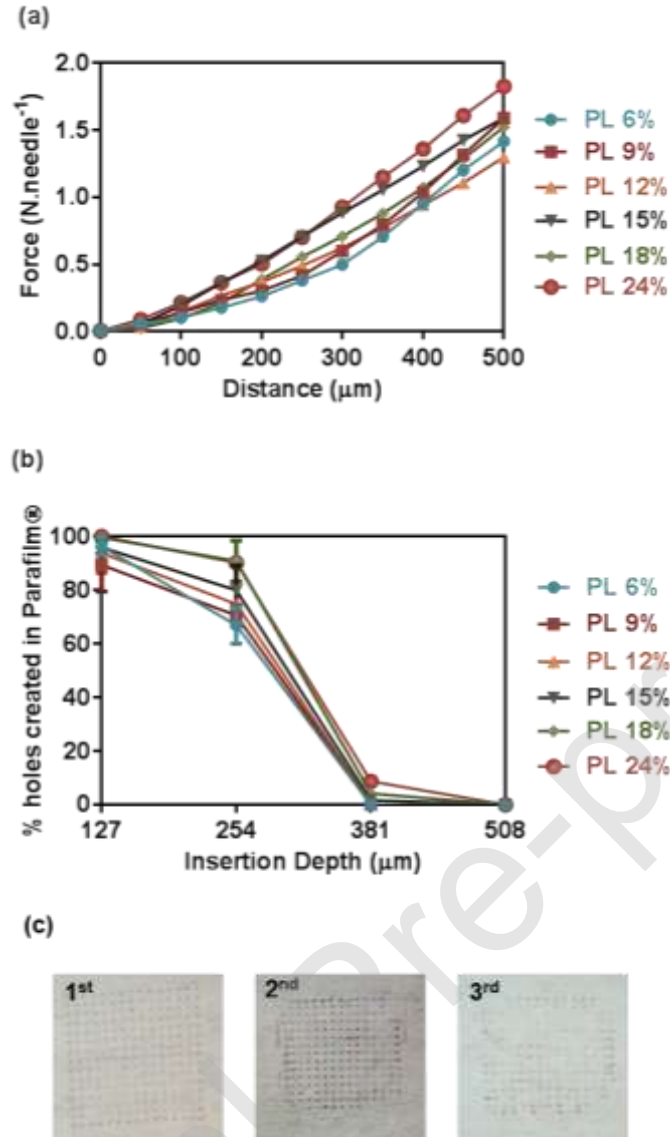
Fig. 3. (a) Force-displacement curves of microneedles fabricated with 6, 9, 12, 15, 18 and 24% (w/v) PL solutions under an axial force load. (b) Insertion of PL microneedles into a polymeric model membrane for skin insertion using Parafilm®. (c) Photos of the first, second and third Parafilm® layer after insertion using PL 24 % MNs.

3.3. Preparation and characterization of insulin-loaded PL dissolving MNs patches

MNs prepared with a PL solution of 24% (w/v) and incorporating 12.4 IU insulin, *i.e.* 0.2 IU insulin *per* kg considering an individual of average body mass of 62 kg (Walpole et al., 2012), produced arrays with a regular and homogeneous morphology

(Fig. 1(b)). Similarly, the mechanical behaviour was comparable to that of the PL MNs without the polypeptide, showing that these needles bend and do not break under an axial force load (Fig.4(a)).

The thermal stability and degradation profiles of the PL 24% and PL 24% + insulin MNs, and pure insulin for comparison purposes, were assessed by TGA (Fig. 4(b)). The thermogram of the pure PL MNs exhibited a pattern of degradation typical of this polysaccharide, as previously reported for PL films (Trovatti, Fernandes, Rubatat, Perez, et al., 2012; Trovatti, Fernandes, Rubatat, Freire, et al., 2012). A single-step weight-loss is observed with a maximum decomposition temperature (Td_{max}) of 294 ℃. At 800 ℃, a residue corresponding to 7% of the original mass of the sample is obtained. Pure insulin displays an initial weight-loss due to water evaporation and the next weight loss, which starts at 230 ℃ and reaches a Td_{max} at 286 ℃, is associated with insulin backbone decomposition (Farahani, Ghasemzaheh, & Afraz, 2016).

The thermogram of PL 24% + Insulin also exhibits a single-step weight-loss with a Td_{max} at 242 ℃. Herein, it is not possible to detect any significant weight-loss in insulin-loaded MNs related to insulin decomposition, which might be due to the low amount of insulin present in the MNs. These results show that the incorporation of insulin into the PL MNs promotes a slight decrease of the thermal stability of PL. However, considering sterilization methods for clinical application, these results show that all PL MNs studied are thermally stable and could resist autoclaving temperatures (*ca*. 120 ℃).
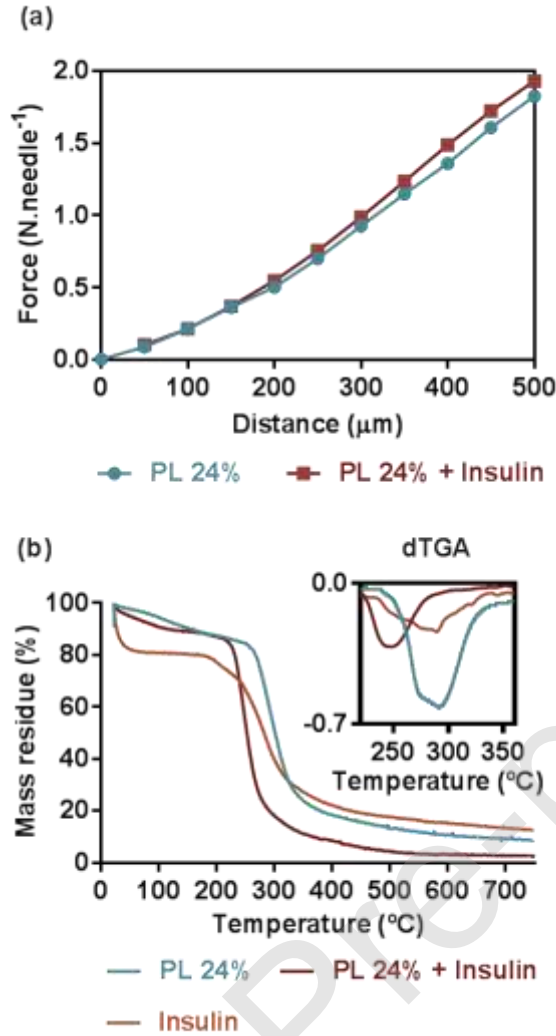
Fig. 4. (a) Force-displacement curves of PL 24% and PL 24% + Insulin microneedles. (b) Thermograms of insulin, and PL 24% and PL 24% + Insulin MNs. Inset displays the derivative plot of the thermogravimetric analysis of these samples.

The hygroscopicity of PL 24% and PL 24% + Insulin MNs patches was evaluated by measuring their weight variation over one week when stored at a relative humidity of 75%. Fig. 5(a) shows the weight gain of these MNs patches, being observed that the weight of both PL MNs patches remained almost unaltered during the first two days and their increase after one week was less than 16%. Moreover, PL-based MNs patches maintained their appearance, which suggests their stability in zones with high humidity

storage conditions. These results are in line with the low hygroscopic nature of PL (Rekha & Sharma, 2007).

FTIR-ATR analysis was performed to assess possible interactions between the PL microneedles and insulin. The FTIR-ATR spectrum of PL (Fig. 5(b)) shows the typical bands of a polysaccharide backbone (Kacuráková, Capek, Sasinková, Wellner, & Ebringerová, 2000). The vibrations around 3305 cm^{-1} are attributed to the OH stretching, whereas those at 2935 and 1250-1460 cm^{-1} are ascribed to CH and CH$_2$ stretching vibrations. The bending motion of adsorbed water (H–O–H) is evidenced at 1650 cm^{-1} and the glycosidic bridges (C–O–C), characteristic of polysaccharides, are observed at 1170-1050 cm^{-1} (Kacuráková et al., 2000). On the other hand, the FTIR-ATR spectrum of insulin displays a peak at 1638 cm^{-1}, corresponding to the amide I vibration. The amide II band is usually observed at 1510-1580 cm^{-1}, representing the in-plane N–H bending and also C–N and C–C stretching vibrations (Arrondo, Muga, Castresana, & Goñi, 1993). After incorporation of insulin into the PL MNs, the spectrum unveils essentially the peaks of the PL matrix. This is certainly due to the low amount of insulin incorporated into the MNs. In addition, no shifts in peaks positions were observed, which indicates that there are no significant interactions between PL and insulin and that PL might be used as a matrix for the safe incorporation of this polypeptide, retaining its structural features.

(a)

(b)

(c)
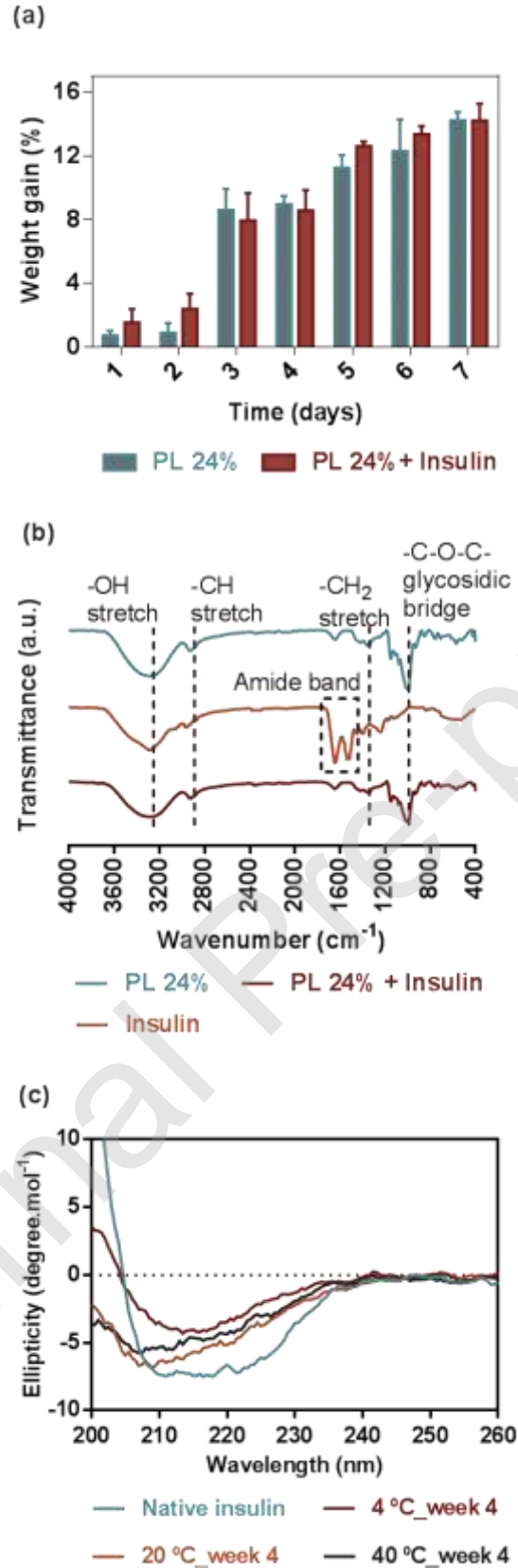
Fig. 5. (a) Weight gain of PL 24% and PL 24% + Insulin MNs when stored at 75% relative humidity for 7 days, (b) FTIR-ATR spectra of insulin, PL 24% and PL 24% +

23

Insulin MNs, and (c) circular dichroism spectra of native insulin and insulin in PL 24% MNs after four weeks of storage at different temperature.

The stability of insulin loaded into the PL MNs was assessed by CD after storage at 4, 20 and 40 ºC for 4 weeks (Fig. 5 (c)). The CD spectra of insulin displays a band at 208 nm and a slight increase at 223 nm, corresponding to the α-helix and β-structures of insulin (Pocker & Biswas, 1980). After storage under different conditions, the CD pattern does not reflect changes in the secondary structure, suggesting that PL 24% + Insulin MNs are stable for at least one month under these storage conditions. The qualitative measurement of the ratio of the bands showed that there is no conformational conversion of insulin (Sun, Zhang, Wu, Zheng, & Li, 2014). Nevertheless, the shift in the wavelength might be associated with the presence of PL in solution. This result agrees with the FTIR-ATR data that suggested poor or no interactions between PL and insulin. Overall, these results indicate that PL MNs allow the incorporation and transport of sensitive biologic drugs such as insulin, under dry conditions, enabling peptide stability without requiring cold chain distribution and storage.

3.4. In vitro skin insertion of insulin-loaded MNs

The skin insertion ratio and depth of the PL and PL 24% + Insulin MNs were assessed by placing the patches on top of *ex vivo* human abdominal skin and pressing with a small probe with a loading force of 40 N for 30 seconds. After applying the axial force load, removing the PL MN patches and applying a dye, the skin surface displayed black spots indicating that the dye was located within the skin (Fig. 6(a)). Histological examination (Fig. 6(b-c)) confirmed skin perforation, with the black dye selectively staining the sites of insertion. The PL 24% + Insulin MNs created puncture sites with an

insertion depth between 40 and 381 μm. These results are comparable with published data, in which starch/gelatin MNs of 600 μm height (50 μm higher than these PL MNs), used also for insulin administration, created skin puncture sites of about 200 μm (Ling & Chen, 2013). The differences in skin insertion depth may be due to natural skin elasticity (Gomaa et al., 2010). Overall, these results reinforce the ability of MNs to cross the *stratum corneum* and epidermis, and reach the dermis layer, using PL as the unique component of the MN arrays.
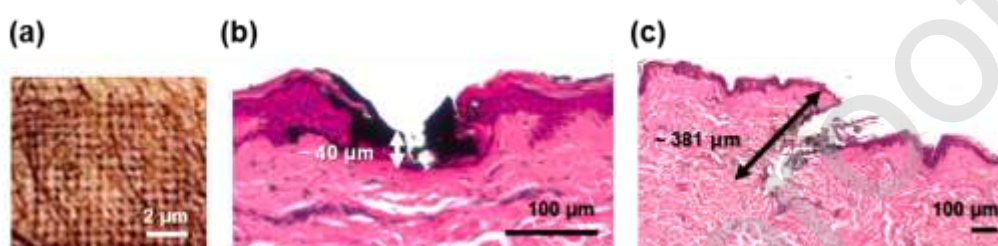

Fig. 6. (a) Photograph of the skin after insertion of PL MNs stained with China ink, and (b-c) histological cross-section of human abdominal skin after piercing by insulin-loaded PL MNs.

3.5. In vitro dissolution of PL MNs and insulin delivery

To evaluate the *in vitro* dissolution of the PL MNs, arrays of PL 24% + Insulin were inserted into *ex vivo* human abdominal skin for 5, 15, 30, 50 and 120 min. After peeling off the MNs patches from the skin, it was observed that they gradually became smaller with increased insertion times. Furthermore, complete needle dissolution was attained 120 min after insertion due to contact with the extracellular matrix.

PL 24% + Insulin MNs exhibited a slow initial insulin release within the first 30 min, followed by a quicker release over time (Fig. 7). The PL dissolution in the first 30 min resulted into a release of 19% of the insulin located at the surface of the needles.

Then, the gradual contact with the extracellular matrix provided a continuous insulin release with approximately 87% released 120 min after insertion.
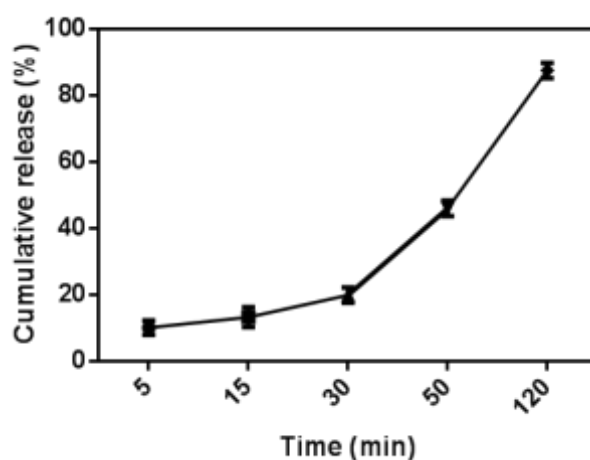

Fig. 7. *In vitro* release of insulin from PL MNs to *ex vivo* human abdominal skin.

3.6. In vitro cytotoxicity assay

Finally, to test the safety of these MNs, the cytotoxicity of pure PL and insulin-loaded PL MNs was evaluated towards human keratinocytes. The results showed that both PL and insulin-loaded polymeric mixtures are non-cytotoxic (Fig. 8), considering that a material is cytotoxic if a reduction of 30% in cell viability is detected (ISO 10993-5:2009(E)). After 2 h of exposure, the time previously determined for needle dissolution using human abdominal skin, all samples (with different amounts of PL MNs) provided normal cell growth values. After 24 h of exposure, a slight decrease in cell viability was achieved when using 150 μg PL *per* well, however, cell viability was still within the non-cytotoxic range.

Overall, these results reinforce the safety of PL for biomedical applications, in particular for MN devices, which disrupt the upper layers of the skin and directly contact with the epidermal and dermal skin layers.
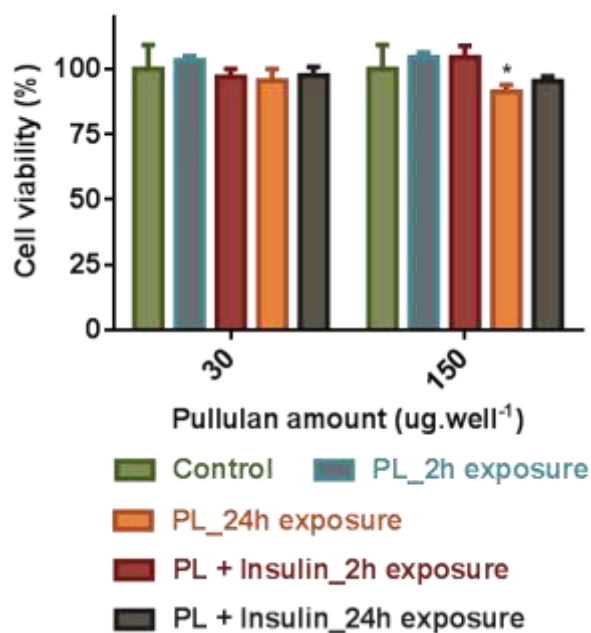
Fig. 8. Viability (%) of human keratinocyte cells exposed to 30 and 150 μg PL *per* well with and without insulin. The data are expressed as mean ± standard deviation of six replicates in each of the two independent experiments. Statistically significant (p<0.05) differences relatively to control are indicated by *.

4. Conclusions

In this work, dissolvable MNs arrays fabricated using PL were prepared for the transdermal administration of insulin. The as-prepared PL MN arrays exhibited good mechanical properties, which enabled the perforation of human skin. In addition, insulin can be incorporated into PL MNs with no changes in its secondary structure for at least one month of storage at 4, 20 and 40 ºC. PL MNs incorporating insulin were evaluated for transdermal delivery, showing that 87% of insulin was released to the skin in the first 120 min. The non-cytotoxic nature of these MNs support their safe use and hence, this work suggests that PL MNs incorporating insulin may in the future be a transdermal alternative to its administration, improving the quality of life of diabetic patients.

27

CRediT authorship contribution statement

Daniela F. S. Fonseca: Investigation, Methodology; Writing - Original Draft, Writing - Review & Editing

Paulo C. Costa: Investigation, Resources, Writing - Review & Editing, Funding acquisition

Isabel F. Almeida: Investigation, Resources, Writing - Review & Editing, Funding acquisition

Patrícia Dias-Pereira: Investigation, Resources, Writing - Review & Editing

Inês Correia-Sá: Resources, Writing - Review & Editing

Verónica Bastos: Investigation, Writing - Review & Editing

Helena Oliveira: Resources, Methodology; Writing - Review & Editing, Funding acquisition

Margarida Duarte-Araújo: Writing - Review & Editing

Manuela Morato: Writing - Review & Editing

Carla Vilela: Investigation, Writing - Review & Editing, Supervision

Armando J. D. Silvestre: Conceptualization, Resources, Writing - Review & Editing, Supervision, Funding acquisition

Carmen S. R. Freire: Conceptualization, Resources, Writing - Review & Editing, Supervision, Funding acquisition

References

Amrita, Arora, A., Sharma, P., & Katti, D. S. (2015). Pullulan-based composite scaffolds for bone tissue engineering: Improved osteoconductivity by pore wall mineralization. *Carbohydrate Polymers*, *123*, 180–189. https://doi.org/10.1016/j.carbpol.2015.01.038

Arrondo, J. L. R., Muga, A., Castresana, J., & Goñi, F. M. (1993). Quantitative studies of the structure of proteins in solution by Fourier-transform infrared spectroscopy. *Progress in Biophysics and Molecular Biology*, *59*(1), 23–56. https://doi.org/10.1016/0079-6107(93)90006-6

Ascenso, A., Pedrosa, T., Pinho, S., Pinho, F., De Oliveira, J. M. P. F., Marques, H. C., … Santos, C. (2016). The Effect of Lycopene Preexposure on UV-B-Irradiated Human Keratinocytes. *Oxidative Medicine and Cellular Longevity*, *2016*, 8214631. https://doi.org/10.1155/2016/8214631

Asche, C. V., Shane-McWhorter, L., & Raparla, S. (2010). Health Economics and Compliance of Vials/Syringes Versus Pen Devices: A Review of the Evidence.

Diabetes Technology & Therapeutics, *12*(S1), S-101-S-108. https://doi.org/10.1089/dia.2009.0180

Bhattacharjee, A., Lopes-da-Silva, J. A., Freire, M. G., Coutinho, J. A. P., & Carvalho, P. J. (2015). Thermophysical properties of phosphonium-based ionic liquids. *Fluid Phase Equilibria*, *400*, 103–113. https://doi.org/10.1016/j.fluid.2015.05.009

Carmo, F., Sathler, P., Zancan, P., Rodrigues, C., Castro, H., de Sousa, V., … Cabral, L. (2014). Therapeutic Nanosystems for Oral Administration of Insulin. *Current Pharmaceutical Biotechnology*, *15*(7), 620–628. https://doi.org/10.2174/1389201015666140915150826

Chen, M.-C., Ling, M.-H., & Kusuma, S. J. (2015). Poly-γ-glutamic acid microneedles with a supporting structure design as a potential tool for transdermal delivery of insulin. *Acta Biomaterialia*, *24*, 106–116. https://doi.org/10.1016/j.actbio.2015.06.021

Chen, M.-C., Ling, M.-H., Lai, K.-Y., & Pramudityo, E. (2012). Chitosan microneedle patches for sustained transdermal delivery of macromolecules. *Biomacromolecules*, *13*(12), 4022–4031. https://doi.org/10.1021/bm301293d

Chen, X., Wang, L., Yu, H., Li, C., Feng, J., Haq, F., … Khan, R. U. (2018). Preparation, properties and challenges of the microneedles-based insulin delivery system. *Journal of Controlled Release*, *288*, 173–188. https://doi.org/10.1016/j.jconrel.2018.08.042

Davis, S. P., Landis, B. J., Adams, Z. H., Allen, M. G., & Prausnitz, M. R. (2004). Insertion of microneedles into skin: Measurement and prediction of insertion force and needle fracture force. *Journal of Biomechanics*, *37*(8), 1155–1163. https://doi.org/10.1016/j.jbiomech.2003.12.010

DeFronzo, R. A., Ferrannini, E., Groop, L., Henry, R. R., Herman, W. H., Holst, J. J.,

… Weiss, R. (2015). Type 2 diabetes mellitus. *Nature Reviews Disease Primers*, *1*, 15019. https://doi.org/10.1038/nrdp.2015.19

Derraik, J. G., Rademaker, M., Cutfield, W. S., Peart, J. M., Jefferies, C., & Hofman, P. L. (2014). Poorer glycaemic control is associated with increased skin thickness at injection sites in children with type 1 diabetes. *Int J Pediatr Endocrinol*, *2014*(1), 2. https://doi.org/10.1186/1687-9856-2014-2

Economidou, S. N., Lamprou, D. A., & Douroumis, D. (2018). 3D printing applications for transdermal drug delivery. *International Journal of Pharmaceutics*, *544*(2), 415–424. https://doi.org/10.1016/j.ijpharm.2018.01.031

Farahani, B. V., Ghasemzaheh, H., & Afraz, S. (2016). Intelligent semi-IPN chitosan-PEG-PAAm hydrogel for closed-loop insulin delivery and kinetic modeling. *RSC Advances*, *6*(32), 26590–26598. https://doi.org/10.1039/c5ra28188a

Fernandes, S. C. M., Sadocco, P., Causio, J., Silvestre, A. J. D., Mondragon, I., & Freire, C. S. R. (2014). Antimicrobial pullulan derivative prepared by grafting with 3-aminopropyltrimethoxysilane: Characterization and ability toformtransparent films. *Food Hydrocolloids*, *35*, 247–252. https://doi.org/10.1016/j.foodhyd.2013.05.014

Fonseca, D. F. S., Vilela, C., Silvestre, A. J. D., & Freire, C. S. R. (2019). A compendium of current developments on polysaccharide and protein-based microneedles. *International Journal of Biological Macromolecules*, *136*, 704–728. https://doi.org/10.1016/j.ijbiomac.2019.04.163

Freire, C., Fonseca, D., Vilela, C., Costa, P., Almeida, I., Pereira, P., & Silvestre, A. (2019). Polysaccharide-based microneedles for transdermal delivery of insulin. In *ABSTRACTS OF PAPERS OF THE AMERICAN CHEMICAL SOCIETY* (Vol. 257). AMER CHEMICAL SOC 1155 16TH ST, NW, WASHINGTON, DC 20036

USA.

Gomaa, Y. A., Morrow, D. I. J., Garland, M. J., Donnelly, R. F., El-Khordagui, L. K., & Meidan, V. M. (2010). Effects of microneedle length, density, insertion time and multiple applications on human skin barrier function: Assessments by transepidermal water loss. *Toxicology in Vitro*, *24*(7), 1971–1978. https://doi.org/10.1016/j.tiv.2010.08.012

Huang, L., Chaurasiya, B., Wu, D., Wang, H., Du, Y., Tu, J., … Sun, C. (2018). Versatile redox-sensitive pullulan nanoparticles for enhanced liver targeting and efficient cancer therapy. *Nanomedicine: Nanotechnology, Biology, and Medicine*, *14*(3), 1005–1017. https://doi.org/10.1016/j.nano.2018.01.015

Ito, Y., Hagiwara, E., Saeki, A., Sugioka, N., & Takada, K. (2006). Feasibility of microneedles for percutaneous absorption of insulin. *European Journal of Pharmaceutical Sciences*, *29*(1), 82–88. https://doi.org/10.1016/j.ejps.2006.05.011

Ito, Y., Yamazaki, T., Sugioka, N., & Takada, K. (2010). Self-dissolving micropile array tips for percutaneous administration of insulin. *Journal of Materials Science: Materials in Medicine*, *21*(2), 835–841. https://doi.org/10.1007/s10856-009-3923-x

Jin, X., Zhu, D. D., Chen, B. Z., Ashfaq, M., & Guo, X. D. (2018). Insulin delivery systems combined with microneedle technology. *Advanced Drug Delivery Reviews*, *127*, 119–137. https://doi.org/10.1016/j.addr.2018.03.011

Kacuráková, M., Capek, P., Sasinková, V., Wellner, N., & Ebringerová, A. (2000). FT-IR study of plant cell wall model compounds: Pectic polysaccharides and hemicelluloses. *Carbohydrate Polymers*, *43*(2), 195–203. https://doi.org/10.1016/S0144-8617(00)00151-X

Larrañeta, E., Moore, J., Vicente-Pérez, E. M., González-Vázquez, P., Lutton, R., Woolfson, A. D., & Donnelly, R. F. (2014). A proposed model membrane and test

method for microneedle insertion studies. *International Journal of Pharmaceutics*, *472*(1–2), 65–73. https://doi.org/10.1016/j.ijpharm.2014.05.042

Lee, J. W., Park, J.-H. H., & Prausnitz, M. R. (2008). Dissolving microneedles for transdermal drug delivery. *Biomaterials*, *29*(13), 2113–2124. https://doi.org/10.1016/j.biomaterials.2007.12.048

Ling, M.-H. H., & Chen, M.-C. C. (2013). Dissolving polymer microneedle patches for rapid and efficient transdermal delivery of insulin to diabetic rats. *Acta Biomaterialia*, *9*(11), 8952–8961. https://doi.org/10.1016/j.actbio.2013.06.029

Liu, S., Jin, M. N., Quan, Y. S., Kamiyama, F., Katsumi, H., Sakane, T., & Yamamoto, A. (2012). The development and characteristics of novel microneedle arrays fabricated from hyaluronic acid, and their application in the transdermal delivery of insulin. *Journal of Controlled Release*, *161*(3), 933–941. https://doi.org/10.1016/j.jconrel.2012.05.030

Matteucci, E., Giampietro, O., Covolan, V., Giustarini, D., Fanti, P., & Rossi, R. (2015). Insulin administration: Present strategies and future directions for a noninvasive (possibly more physiological) delivery. *Drug Design, Development and Therapy*, *9*, 3109–3118. https://doi.org/10.2147/DDDT.S79322

McAllister, D. V, Wang, P. M., Davis, S. P., Park, J.-H. J.-H., Canatella, P. J., Allen, M. G., & Prausnitz, M. R. (2003). Microfabricated needles for transdermal delivery of macromolecules and nanoparticles: fabrication methods and transport studies. *Proceedings of the National Academy of Sciences*, *100*(24), 13755–13760. https://doi.org/10.1073/pnas.2331316100

Mishra, B., Suneetha, V., & Rath, K. (2011). The role of microbial pullulan, a biopolymer in pharmaceutical approaches: A review. *Journal of Applied Pharmaceutical Science*, *1*(6), 45–50.

Mosmann, T. (1983). Rapid colorimetric assay for cellular growth and survival: Application to proliferation and cytotoxicity assays. *Journal of Immunological Methods*, *65*(1–2), 55–63. https://doi.org/10.1016/0022-1759(83)90303-4

Narayan, R. J. (2014). Transdermal delivery of insulin via microneedles. *Journal of Biomedical Nanotechnology*, *10*(9), 2244–2260. https://doi.org/10.1166/jbn.2014.1976

Ogurtsova, K., da Rocha Fernandes, J. D., Huang, Y., Linnenkamp, U., Guariguata, L., Cho, N. H., … Makaroff, L. E. (2017). IDF Diabetes Atlas: Global estimates for the prevalence of diabetes for 2015 and 2040. *Diabetes Research and Clinical Practice*, *128*, 40–50. https://doi.org/10.1016/j.diabres.2017.03.024

Park, J.-H. H., Allen, M. G., & Prausnitz, M. R. (2005). Biodegradable polymer microneedles: Fabrication, mechanics and transdermal drug delivery. *Journal of Controlled Release*, *104*(1), 51–66. https://doi.org/10.1016/j.jconrel.2005.02.002

Pocker, Y., & Biswas, S. B. (1980). Conformational Dynamics of Insulin in Solution. Circular Dichroic Studies. *Biochemistry*, *19*(22), 5043–5049. https://doi.org/10.1021/bi00563a017

Rekha, M. R., & Sharma, C. P. (2007). Pullulan as a promising biomaterial for biomedical applications: A perspective. *Trends in Biomaterials and Artificial Organs*, *20*(2), 111–116.

Ross, S., Scoutaris, N., Lamprou, D., Mallinson, D., & Douroumis, D. (2015). Inkjet printing of insulin microneedles for transdermal delivery. *Drug Delivery and Translational Research*, *5*(4), 451–461. https://doi.org/10.1007/s13346-015-0251-1

Rydén, A., Rstadius, E. S., Bergenheim, K., Romanovschi, A., Thorén, F., Witt, E. A., & Sternhufvud, C. (2016). The humanistic burden of Type 1 Diabetes Mellitus in Europe: Examining health outcomes and the role of complications. *PLoS ONE*,

11(11). https://doi.org/10.1371/journal.pone.0164977

Saffran, M., Pansky, B., Budd, G. C., & Williams, F. E. (1997). Insulin and the gastrointestinal tract. *Journal of Controlled Release*, *46*(1–2), 89–98. https://doi.org/10.1016/S0168-3659(96)01578-7

Shah, R., Patel, M., Maahs, D., & Shah, V. (2016). Insulin delivery methods: Past, present and future. *International Journal of Pharmaceutical Investigation*, *6*(1), 1. https://doi.org/10.4103/2230-973x.176456

Silva, N. H. C. S., Vilela, C., Almeida, A., Marrucho, I. M., & Freire, C. S. R. (2017). Pullulan-based nanocomposite films for functional food packaging: Exploiting lysozyme nanofibers as antibacterial and antioxidant reinforcing additives. *Food Hydrocolloids*, *77*, 921–930. https://doi.org/10.1016/j.foodhyd.2017.11.039

Singh, Ram S., Saini, G. K., & Kennedy, J. F. (2008). Pullulan: Microbial sources, production and applications. *Carbohydrate Polymers*, *73*(4), 515–531. https://doi.org/10.1016/j.carbpol.2008.01.003

Singh, Ram Sarup, Kaur, N., Rana, V., & Kennedy, J. F. (2016). Recent insights on applications of pullulan in tissue engineering. *Carbohydrate Polymers*, *153*, 455–462. https://doi.org/10.1016/j.carbpol.2016.07.118

Singh, Ram Sarup, Kaur, N., Rana, V., & Kennedy, J. F. (2017, September 1). Pullulan: A novel molecule for biomedical applications. *Carbohydrate Polymers*. Elsevier. https://doi.org/10.1016/j.carbpol.2017.04.089

Sun, L., Zhang, X., Wu, Z., Zheng, C., & Li, C. (2014). Oral glucose- and pH-sensitive nanocarriers for simulating insulin release in vivo. *Polymer Chemistry*, *5*(6), 1999–2009. https://doi.org/10.1039/c3py01416a

Suneetha, V., Sindhuja, K. V, & Singh, S. K. (2010). Screening and characterization of pullulan producing microorganism from plant leaves in Chittoor district. *Asian*

Journal of Microbiology, Biotechnology and Environmental Sciences, *12*(1), 149–155. Retrieved from https://www.researchgate.net/publication/281233626

Tao, X., Tao, T., Wen, Y., Yi, J., He, L., Huang, Z., … Yang, X. (2018). Novel Delivery of Mitoxantrone with Hydrophobically Modified Pullulan Nanoparticles to Inhibit Bladder Cancer Cell and the Effect of Nano-drug Size on Inhibition Efficiency. *Nanoscale Research Letters*, *13*(1), 345. https://doi.org/10.1186/s11671-018-2769-x

Trovatti, E., Fernandes, S. C. M. M., Rubatat, L., Perez, D. da S., Freire, C. S. R. R., Silvestre, A. J. D. D., & Neto, C. P. (2012). Pullulan-nanofibrillated cellulose composite films with improved thermal and mechanical properties. *Composites Science and Technology*, *72*(13), 1556–1561. https://doi.org/10.1016/j.compscitech.2012.06.003

Trovatti, E., Fernandes, S. C. M., Rubatat, L., Freire, C. S. R., Silvestre, A. J. D., & Neto, C. P. (2012). Sustainable nanocomposite films based on bacterial cellulose and pullulan. *Cellulose*, *19*(3), 729–737. https://doi.org/10.1007/s10570-012-9673-9

Trovatti, E., Silva, N. H. C. S., Duarte, I. F., Rosado, C. F., Almeida, I. F., Costa, P., … Neto, C. P. (2011). Biocellulose membranes as supports for dermal release of lidocaine. *Biomacromolecules*, *12*(11), 4162–4168. https://doi.org/10.1021/bm201303r

Tuomi, T., Santoro, N., Caprio, S., Cai, M., Weng, J., & Groop, L. (2014). The many faces of diabetes: A disease with increasing heterogeneity. *The Lancet*, *383*(9922), 1084–1094. https://doi.org/10.1016/S0140-6736(13)62219-9

Walpole, S. C., Prieto-Merino, D., Edwards, P., Cleland, J., Stevens, G., & Roberts, I. (2012). The weight of nations: An estimation of adult human biomass. *BMC Public*

Health, *12*(1), 439. https://doi.org/10.1186/1471-2458-12-439

Yu, W., Jiang, G., Zhang, Y., Liu, D., Xu, B., & Zhou, J. (2017). Polymer microneedles fabricated from alginate and hyaluronate for transdermal delivery of insulin. *Materials Science and Engineering C*, *80*, 187–196. https://doi.org/10.1016/j.msec.2017.05.143

Zhang, Y., Jiang, G., Yu, W., Liu, D., & Xu, B. (2018). Microneedles fabricated from alginate and maltose for transdermal delivery of insulin on diabetic rats. *Materials Science and Engineering C*, *85*, 18–26. https://doi.org/10.1016/j.msec.2017.12.006